Research Square

Preprints are preliminary reports that have not undergone peer review.
They should not be considered conclusive, used to inform clinical practice,
or referenced by the media as validated information.

Interfacial Strengthening and Stress Mitigation in GH4169/Ti60 Diffusion-Bonded Joints Driven by Cu Interlayer Thickness Design

Shibo Zhu
Henan University of Science and Technology School of Materials Science and Engineering
Zhuoli Yu
Henan University of Science and Technology School of Materials Science and Engineering
Sen Yang
Henan University of Science and Technology School of Materials Science and Engineering
Kaiyang Zhang
Henan University of Science and Technology School of Materials Science and Engineering
Tao Jiang
Henan University of Science and Technology School of Materials Science and Engineering
Qi Gao
Luoyang Ship Material Research Institute
Yanan Zhang
Jonhon Optronic Technology Co Ltd
Li Ma
Jonhon Optronic Technology Co Ltd
Liangliang Zhang
Henan Polytechnic University School of Materials Science and Engineering
Xingxing Wang
North China University of Water Resources and Electric Power
Zhiqian Liao
Luoyang Ship Material Research Institute
Ranfeng Qiu
Henan University of Science and Technology School of Materials Science and Engineering
Hua Yu
kedayuhua@126.com

Henan University of Science and Technology https://orcid.org/0000-0002-3373-6300

Research Article

Keywords: GH4169

Posted Date: November 11th, 2026

DOI: https://doi.org/10.21203/rs.3.rs-11249178/v1

License: This work is licensed under a Creative Commons Attribution 4.0 International License.
Read Full License

Interfacial Strengthening and Stress Mitigation in GH4169/Ti60 Diffusion-Bonded Joints Driven by Cu Interlayer Thickness Design

Shibo Zhu [a], Zhuoli Yu [a,1], Sen Yang [a], Kaiyang Zhang [a], Tao Jiang [a], Qi Gao [b], Yanan Zhang [c], Li Ma [c], Liangliang Zhang [d], Xingxing Wang [e], Zhiqian Liao [b,*], Ranfeng Qiu [a,], Hua Yu [a,f,***]**

[a] *School of Material Science & Engineering, Henan University of Science and Technology, Luoyang, 471000, China*

[b] *Luoyang Ship Material Research Institute, Luoyang, 471023, China*

[c] *Jonhon Optronic Technology Co Ltd, Luoyang, 471000, China*

[d] *School of Material Science & Engineering, Henan Polytechnic University, Jiaozuo, 454003*

[e] *Henan International Joint Laboratory of High-efficiency Special Green Welding, North China University of Water Resources and Electric Power,Zhengzhou 450045, China*

[f] *Longmen Laboratory, Luoyang, 471000, China*

[*] Corresponding author. Luoyang Ship Material Research Institute, Luoyang, 471023, China

[**] Corresponding author. School of Material Science & Engineering, Henan University of Science and Technology, Luoyang, 471000, China

[***] Corresponding author. School of Material Science & Engineering, Henan University of Science and Technology, Luoyang, 471000, China

E-mail addresses: lzq0379@163.com (Zhiqian Liao), qiurf1221@163.com (Ranfeng Qiu), kedayuhua@126.com (Hua Yu).

[1] These authors contributed equally to this work and should be considered co-first authors.

Acknowledgements

This work is supported by The Science and Technology Innovation Leading Talent Support Program of Henan Province (26420050001）

Abstract

Heterogeneous joining of GH4169 Ni-based superalloy and Ti60 titanium alloy combines their advantages, but brittle Ti-Ni phases and stress concentration lower joint strength. Here, pure Cu interlayers were used for diffusion bonding GH4169/Ti60 joints. The Cu foil thickness was varied to study microstructural evolution and reveal strengthening and fracture mechanisms. Direct TLP bonding produces a joint comprising diffusion layer I (GH4169 side), central brazing seam II, and diffusion layer III (Ti60 side), with typical microstructure GH4169/Cr_{ss}+$(Ni,Cr,Fe)_{ss}$/TiNi/Ti_2Ni/α-Ti/Ti60; brittle TiNi compounds degrade performance. With Cu foil, the typical microstructure becomes Ti(Ni,Cu)/TiCu+TiAl/β-Ti+Ti_3Sn/α-Ti+Ti_2Cu/α-Ti/Ti60. Increasing Cu thickness coarsens zone II grains and reduces the high-angle grain boundary fraction from 92.5% to 46.1%. At 0.03mm Cu, the maximum KAM values in zones I, II, and III are 4.88°, 4.99°, and 4.97°, respectively, indicating relatively uniform stress. The $(Ni,Cu)_{ss}$/Ti_3Sn/Ti–Cu layered structure in zone II greatly relieves residual stress and gives a maximum joint strength of 190MPa. Fracture morphology and path indicate brittle fracture; cracks initiate between the $(Cu,Ni)_{ss}$ and TiCu phases and form small secondary cracks.

Keywords：

GH4169;
Ti60;
Cu foil;
Transient Liquid Phase Welding;
Microstructure

1. Introduction

Heterogeneous material joining structures can fully exploit the excellent properties of different materials to meet the requirements of various service conditions[1]. GH4169 is a nickel-based superalloy widely used in turbine disks, blades, and high-temperature components of rocket engines owing to its excellent high-temperature strength and oxidation resistance[2,3]. Ti60 titanium alloy possesses high specific strength, excellent heat resistance, and low density, making it a promising candidate for structural components in aero-engines. The density of Ti60 alloy (4.50-4.57 g/cm³) is only about 55% that of GH4169 superalloy (8.24 g/cm³). Therefore, replacing GH4169 superalloy with Ti60 alloy can reduce the weight of aero-engines and effectively improve the thrust-to-weight ratio[4]. However, the significant differences in physicochemical properties between Ni-based superalloys and titanium alloys can lead to defects such as cracks in Ti/Ni joints, and brittle intermetallic compounds (IMCs) readily form at the joint, making the selection of an appropriate joining method and transition interlayer crucial.

At present, the main methods for joining Ti/Ni dissimilar alloys include fusion welding, brazing, and diffusion bonding[5–7]. Fusion welding achieves joint formation through melting of the base metals, mutual dissolution, and subsequent solidification upon cooling; however, the relatively high heating and cooling rates and localized heating can induce large residual thermal stresses and crack formation in the joint. Moreover, brittle intermetallic compounds such as Ti_2Ni, TiNi, and $TiNi_3$ readily form between Ti and Ni at elevated temperatures, deteriorating joint performance[8,9]. Brazing, as a uniform heating process, allows the base metals and interlayer to be heated evenly, effectively reducing thermal stress concentration and thus serving as an effective method for dissimilar metal joining. Diffusion bonding requires applying a certain load to the base metals to ensure sufficient atomic interdiffusion, thereby enabling high-strength dissimilar metal joints. Brazing or diffusion bonding can produce relatively superior joints for Ti/Ni dissimilar alloys. Transient liquid phase (TLP) bonding combines the characteristics of both brazing and diffusion bonding. In this process, one or more interlayer metals (similar to filler metals) are placed between dissimilar base metals, and the solid-liquid interface formed after interlayer melting enables interdiffusion and dissolution of dissimilar metals, resulting in a joint[10–12]. This joining process not only alleviates the physicochemical mismatch between base metals through the interlayer but also provides the high joint strength characteristic of diffusion bonding.

He et al.[13] employed Ni foil as an interlayer to diffusion-bond a high-niobium β-γ TiAl alloy (HNBG) to a Ni-based superalloy (IN718). The phase constitution of the joint was IN718/γ-Ni/γ′-Ni_3(Al, Ti)/τ4-Ni_2AlTi/τ3-$NiAl_3Ti_2$/β/B2 + τ3-$NiAl_3Ti_2$/HNBG. Under 850°C × 20min × 20MPa, a maximum shear strength of 346MPa was obtained for the HNBG/Ni/IN718 joint. The introduction of the Ni interlayer significantly improved the elemental distribution and microstructure, increasing the shear strength of the HNBG/Ni/IN718 joint by 34.6% compared with that of the joint without any interlayer. When the bonding temperature was below 850°C, shear fracture mainly occurred in the γ′ diffusion layer, and the fracture mode was brittle

transcrystalline fracture.

Wang et al.[14] achieved vacuum brazing between a selective laser melting (SLM)-fabricated TC4 titanium alloy and an Inconel718 superalloy using a Ti-Zr-Cu-Ni amorphous brazing filler. The microstructure of the joint was mainly composed of TC4 base metal / Widmanstätten structure / β-Ti + Ti_2Cu / $(Ti, Zr)_2(Cu, Ni)$ / $(Ti, Zr)_2(Cu, Ni)$ + α-Ti / Fe_2Ti + Cr_7Ni_3 + $TiNi_3$ + Ni(Fe, Cr) solid solution / Inconel718 base metal. At a brazing temperature of 930°C and a brazing time of 20min, the joint exhibited the best performance, with an average shear strength of 111.2MPa. Cracks initiated in the $(Ti, Zr)_2(Cu, Ni)$ and $(Ti, Zr)_2(Cu, Ni)$ + α-Ti two-phase zone and propagated within this region. The fracture mode was brittle fracture, and the mechanical properties of the joint were dominated by Ti-based intermetallic compounds.

In summary, owing to the differences in physical and chemical properties between Ti and Ni, welded joints often suffer from large residual stresses, and the formation of Ti-Ni IMCs severely degrades joint strength. According to the Ni-Cu binary phase diagram, Ni and Cu can form a continuous solid solution. The addition of Cu foil promotes the dissolution of Ni into the solid solution, thereby reducing the formation of brittle TiNi compounds; moreover, the high plasticity of Cu can alleviate thermal stress mismatch between Ti and Ni[8]. Therefore, this study proposes the use of a pure Cu interlayer for diffusion bonding of GH4169 nickel-based superalloy and Ti60 titanium alloy, with the amount of Cu controlled by adjusting the Cu foil thickness, to obtain high-strength GH4169/Ti60 dissimilar alloy joints. The effects of the Cu foil thicknesses on the microstructure and shear strength of the diffusion-bonded joints were investigated, the relationship between mechanical properties and microstructure was established, and the strengthening and fracture mechanisms of the diffusion-bonded joints were elucidated.

2. Experimental Materials and Methods

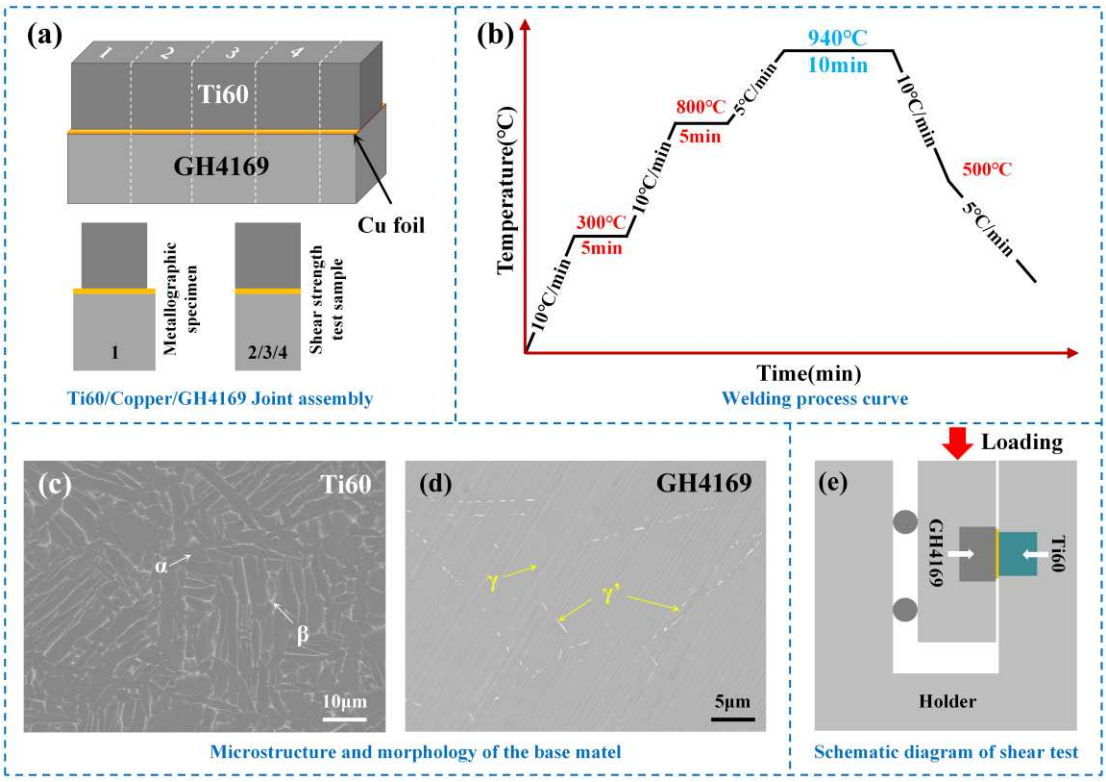


Figure 1. (a) Schematic diagram of Ti60/GH4169 joint assembly, (b) Welding process curve, (c) Microstructure of Ti60 alloy, (d) Microstructure of GH4169 alloy, (e) Schematic diagram of shear test

The base metals used in this study were Ti60 titanium alloy and GH4169 nickel-based superalloy. The chemical compositions of the base metals are listed in Table 1, and Figure 1(c) and (d) show the microstructures of Ti60 and GH4169, respectively. Prior to the experiments, the two base metals were cut into dimensions of 30mm × 6mm × 5mm and 30mm × 5mm × 5mm, respectively, by wire electrical discharge machining. Pure Cu foils with thicknesses of 0, 0.01mm, 0.03mm, 0.05mm, and 0.1mm were used as interlayers for diffusion bonding. Before diffusion bonding, the base metals and Cu interlayers were ground with SiC abrasive papers to remove surface oxide layers and then ultrasonically cleaned in anhydrous ethanol for 10min. The base metals and interlayer were assembled in a butt configuration, as shown in Figure 1(a).

The bonding temperature was selected mainly based on the eutectic point of the compounds formed by metallurgical reactions during bonding. The lowest eutectic point of the Ti-Cu system is 880℃, and the optimal diffusion bonding temperature is typically 50-60℃ above the eutectic reaction temperature[15,16]; therefore, bonding was performed at 940℃ in this study. Under a vacuum of less than 5×10^{-3}Pa, the samples were heated to 940℃ at a rate of 15℃/min and held for 10min under a pressure of 10MPa. After bonding, the samples were cooled to 500℃ at a rate of 10℃/min and then furnace-cooled to room temperature. The bonding thermal cycle is shown in Figure 1(b).

After diffusion bonding, the joints were machined into specimens for microstructural observation and shear property testing, as illustrated in Figure 1(a). The shear strength of the joints was tested using the fixture shown in Figure 1(e). The microstructure and fracture morphology of the joints were characterized by scanning electron microscopy (SEM), energy-dispersive spectroscopy (EDS), and electron backscatter diffraction (EBSD). EBSD specimens were prepared by argon ion polishing. The fracture path and fracture morphology were characterized by SEM.

Table 1. Chemical composition of base metal (wt%)

Base metal	Ti	Al	Sn	Ni	Cr	Fe	Nb	Zr	Mo
GH4169	0.83	0.45	-	52.40	18.20	Bal.	4.98	-	2.95
Ti60	Bal.	5.70	4.00	-	-	-	0.40	3.5	0.40

3. Results and Discussion

3.1 Typical microstructure of the joint

Figure 2(a) shows the typical microstructure of the GH4169/Ti60 joint diffusion bonded at 940℃ for 10 min without an interlayer. The joint can be divided into three zones: diffusion layer I adjacent to the GH4169 side, central brazing seam II, and diffusion layer III adjacent to the Ti60 side. Figure 2(b) presents a magnified view of the marked region in Figure 2(a). It can be seen that obvious cracks appear in the central brazing seam II of the joint. The cracks initiate from the gray phase in Zone II and gradually propagate into diffusion layer I, indicating that the base metals were not well bonded. Diffusion layer I is mainly composed of alternately distributed white and light gray acicular phases. According to the EDS analysis results of Points 5 and 6 in Figure 2(b), this region is inferred to be mainly $(Ni,Cr,Fe)_{ss}$, suggesting that only the diffusion of Ni into Ti60 occurred here.

Zone II is the central brazing seam and consists mainly of a gray phase. EDS analysis results show that the main elements at Points 1 and 4 are Ti and Ni. The atomic ratios of Ti to Ni at Points 1 and 4 are approximately 2:1 and 1:1, respectively, as listed in Table 2. Combined with the Ti-Ni binary phase diagram, these phases are inferred to be Ti_2Ni and TiNi. Owing to the different interdiffusion rates of Ni and Ti, the variation in Ni content leads to the formation of Ti_2Ni and TiNi phases in Zone II[17]. The lattice parameter mismatch between Ti_2Ni and α-Ti is large ($a_{Ti2Ni}\approx1.128$nm, $a_{\alpha\text{-}Ti}\approx0.296$nm), whereas the mismatch between Ti_2Ni and TiNi is relatively small. The thermal stress concentration generated during cooling after bonding preferentially causes cracks to initiate between the Ti_2Ni and α-Ti phases and then propagate to the interface between Ti_2Ni and TiNi, which is consistent with the crack propagation phenomenon shown in Figure 2.

Diffusion layer III is mainly composed of a dark gray matrix phase with uniformly distributed light gray phases. EDS results show that the main element at Point 3 is Ti, similar to the composition of the base metal, and it is inferred to be α-Ti. In summary, the typical interfacial microstructure of the joint without any interlayer is GH4169/Cr_{ss} + $(Ni,Cr,Fe)_{ss}$/TiNi/Ti_2Ni/α-Ti/Ti60.

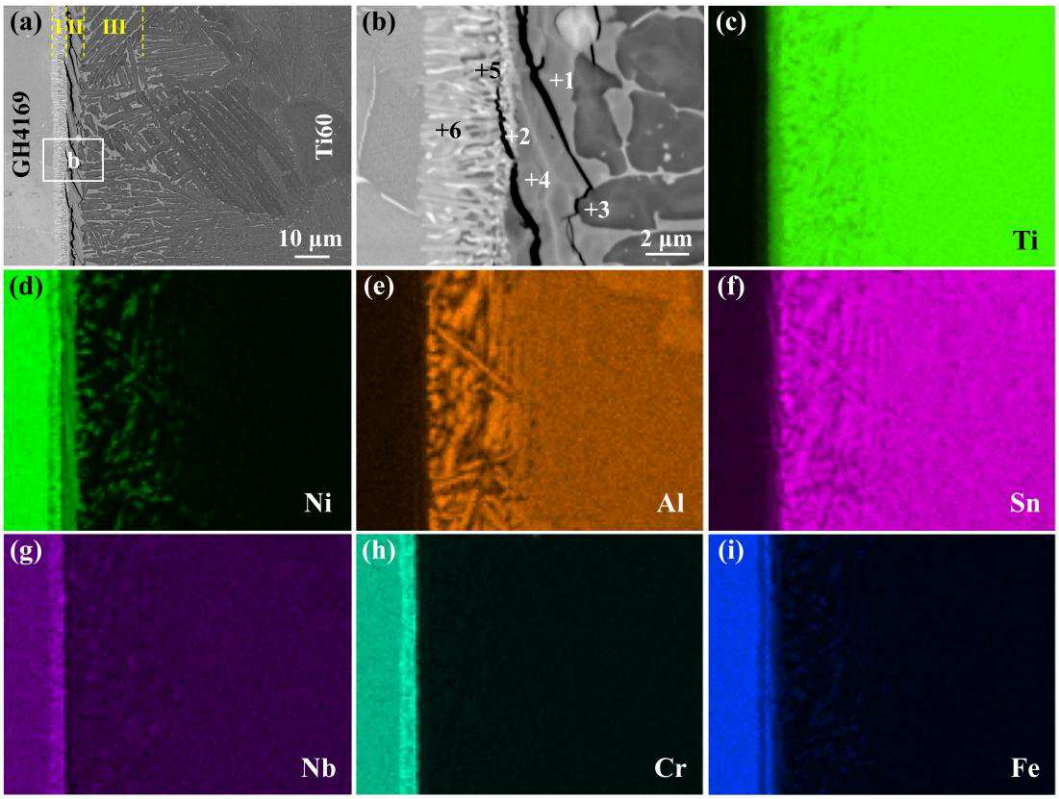


Figure 2. (a) the interface microstructure of the GH4169/Ti60 diffusion bonding joint without interlayer; (b) enlarged view of the marked area in (a)

Table 2. EDS point analysis results at the marked location in Figure 2(b)

Point	Al	Ti	Cr	Fe	Ni	Nb	Possible Phase
1	3.25	58.54	0.78	4.72	30.29	0.13	Ti_2Ni
2	3.84	24.87	16.2	30.04	14.77	3.69	$TiNi+(Ni,Cr,Fe)_{ss}$
3	10.78	84.99	0.2	0	0.77	0.46	α-Ti
4	2.78	43.3	1.62	13.46	35.93	0.18	TiNi
5	0.93	7.55	58.15	13.22	14.63	2.39	$Cr_{ss}+(Ni,Cr,Fe)_{ss}$
6	1.1	3.41	37.94	26.67	24.39	2.41	$(Ni,Cr,Fe)_{ss}$

The morphology of the GH4169/Ti60 joint diffusion bonded at 940°C for 10min with a 0.03mm thick Cu foil interlayer is shown in Figure 3(b). Compared with the joint without any interlayer, the microstructure is sound and free of defects such as cracks and voids. Figure 3(a) and (c) show magnified views of the diffusion layers in Figure 3(b). EDS analysis is performed on phases with different contrasts in the brazing seam, and the chemical compositions of the marked positions are listed in Table 3.

As shown in Figure 3(b), the central brazing seam mainly consists of a light gray phase layer, a gray phase layer, and white blocky phases precipitated between the two layers. The light gray phase at Point 1 is mainly composed of Ti, Ni, and Cu. Since both Cu and Ni have face-centered

cubic (FCC) structures with similar atomic sizes and are completely miscible with each other[18], and elemental mapping shows that Cu and Ni are distributed at the same locations, the light gray phase at Point 1 is inferred to be Ti(Ni,Cu). Based on the EDS results of Points 2 and 3 in Table 3, the gray blocky phases are inferred to be TiCu and TiAl phases. Point 4 marks the white blocky phase in the central brazing seam, with a Sn content of 19.22 at.%. Combined with the Ti–Sn binary phase diagram, this phase is inferred to be a (β-Ti + Ti_3Sn) eutectic structure[19].

The gray structure at Point 5 is located in the diffusion layer between the brazing seam and Ti60, and it mainly contains Ti and Al; therefore, it is inferred to be α-Ti. Point 6 marks the light gray network structure in the diffusion layer on the Ti60 side. According to the atomic ratio of Ti to Cu, this phase is considered to be α-Ti + Ti_2Cu, which results from interdiffusion between molten Cu foil and Ti from the Ti60 substrate. The typical interfacial microstructure of the joint is GH4169/Ti(Ni,Cu)/TiCu + TiAl/β-Ti + Ti_3Sn/α-Ti + Ti_2Cu/α-Ti/Ti60.

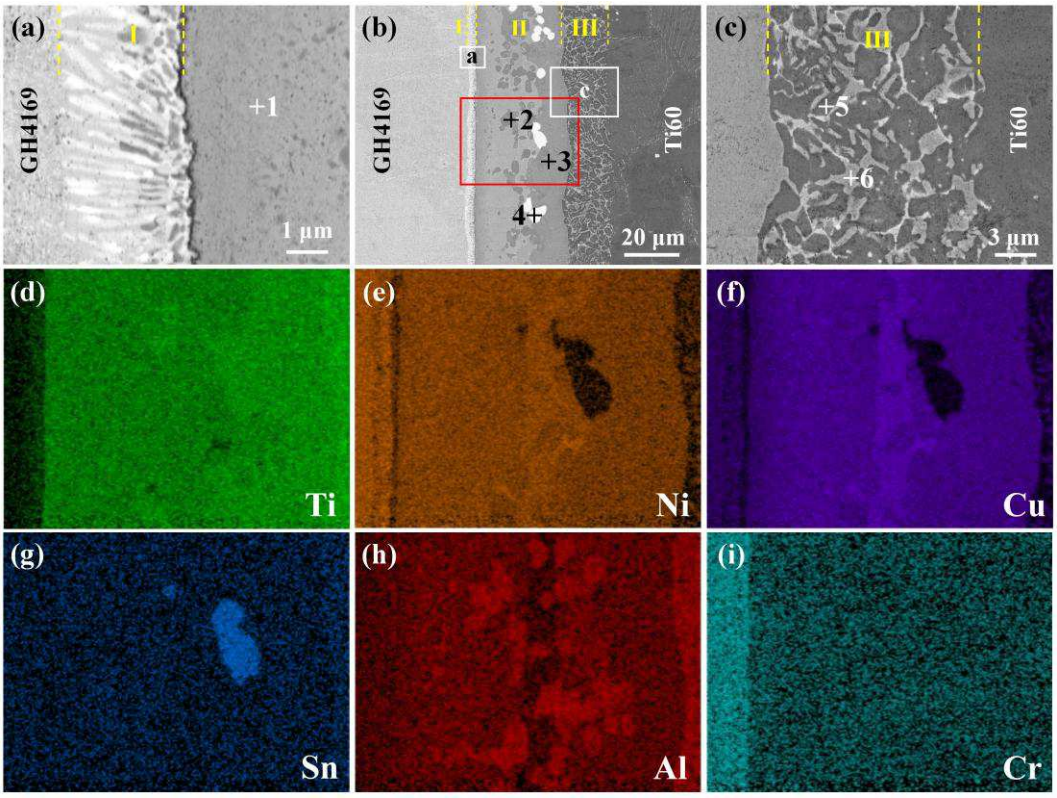


Figure 3. Microstructure morphology of GH4169/Ti60 joint diffusion bonded using 0.03mm Cu foil

Table 3. EDS point analysis results at the marked location in Figure 3

Point	Al	Ti	Cr	Fe	Ni	Cu	Sn	Nb	Possible phase
1	3.1	43.57	2.67	9.7	21.07	18.6	1.01	0.28	Ti(Ni,Cu)
2	14.57	46.28	0.2	0.4	1.86	35.47	0.79	0.43	TiCu+TiAl
3	14.78	48.34	0	0.12	0.34	35.9	0.41	0.11	TiCu+TiAl

4	5.48	71.53	0.8	0.2	0.15	1.89	19.22	0.73	β-Ti+Ti_3Sn
5	14.4	81.89	0	0	0	2.07	1.22	0.42	α-Ti
6	5.32	65.58	0.51	0.07	4.36	22.69	1.27	0.2	α-Ti+Ti_2Cu

Line scan analysis was performed on the diffusion-bonded joint with a 0.03mm thick Cu foil interlayer, as shown in Figure 4. The Ni concentration exhibits a gradual decreasing trend from the GH4169 side toward the Ti60 side, while the Ti concentration also decreases gradually from Ti60 toward the brazing seam. Meanwhile, the variations of Cu and Ni show similar trends, indicating that the addition of Cu foil promotes the solid solution of Ni therein, hinders direct interdiffusion between Ti and Ni, and avoids the formation of brittle Ti-Ni phases. As shown in **Error! Reference source not found.**Figure 3 and Figure 4, white blocky phases precipitated in the brazing seam and exhibited Sn enrichment. This is because during bonding at 940℃, Sn was released from the Ti60 substrate and diffused into the brazing seam. Cu is a β-stabilizing element; while forming Ti_2Cu and TiCu phases with Ti, it also promotes the transformation of α-Ti to β-Ti, thereby increasing the solid solubility of Sn in the β phase. Upon completion of bonding, Sn precipitated from the β phase in the form of Ti_3Sn as a supersaturated phase during cooling[20].

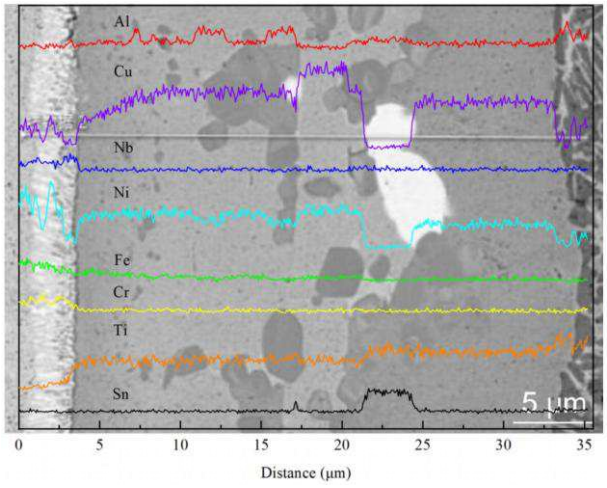


Figure 4. Elemental line scan results of GH4169/Ti60 joint diffusion bonded using 0.03mm Cu foil

3.2 Effect of Cu foil thickness on joint microstructure

Figure 5 shows the microstructures of GH4169/Ti60 joints bonded at 940℃ for 10 min with different Cu foil thicknesses. As shown in Figure 5(a), when no interlayer is added, obvious cracks appear in the diffusion layer of the brazing seam and propagate toward the Ti60 side. Based on the previous analysis, crack initiation occurs mainly between the Ti_2Ni and TiNi phases in the diffusion layer.

With the addition of Cu foils of different thicknesses (0.01 mm, 0.03 mm, 0.05 mm, and 0.1 mm), sound joints are obtained without cracks or voids. The brazing seam width increases with increasing Cu foil thickness, whereas the diffusion layer width remains essentially

unchanged[21]. The addition of Cu hinders direct interdiffusion between Ni and Ti, thereby greatly reducing the formation of continuous brittle Ti-Ni compounds. A small amount of Ti-Cu compounds form at the Ti/Cu interface, while Ni and Cu form ductile $(Ni,Cu)_{ss}$[22]. As a result, the joint exhibits a graded phase-layer structure of GH4169/$(Ni,Cr,Fe)_{ss}$/$(Ni,Cu)_{ss}$/Ti_3Sn/Ti-Cu IMCs/Ti60, which improves the overall ductility of the joint compared with the case without a Cu interlayer. When the Cu foil thickness is 0.05mm, as shown in Figure 5(d), the amount of white phases in the brazing seam increases compared with those with 0.01mm and 0.03mm Cu foils, and the thickness of the dark gray phase in the brazing seam increases. Based on the previous analysis, the increased Cu thickness provides more diffusion space for Ti, leading to an increased fraction of the TiCu phase. Sn also precipitates from the supersaturated β phase in the form of Ti_3Sn during cooling. Nevertheless, the brazing seam still maintains the layered structure of GH4169/$(Ni,Cu)_{ss}$/Ti_3Sn/Ti-Cu/Ti60. Figure 5(e) shows the joint microstructure when the Cu foil thickness reaches 0.1mm. The thickness of the dark gray phase reaches its maximum and extends beyond the white phase in the central brazing seam. At this point, the fractions of TiCu and Ti_2Cu phases in the central brazing seam and the diffusion layer near the GH4169 side also increase. The original layered phase distribution is disrupted, and TiCu, Ti_2Cu, and Ti_3Sn phases together form brittle compound clusters, causing stress concentration in the brazing seam and potentially inducing crack initiation[23].

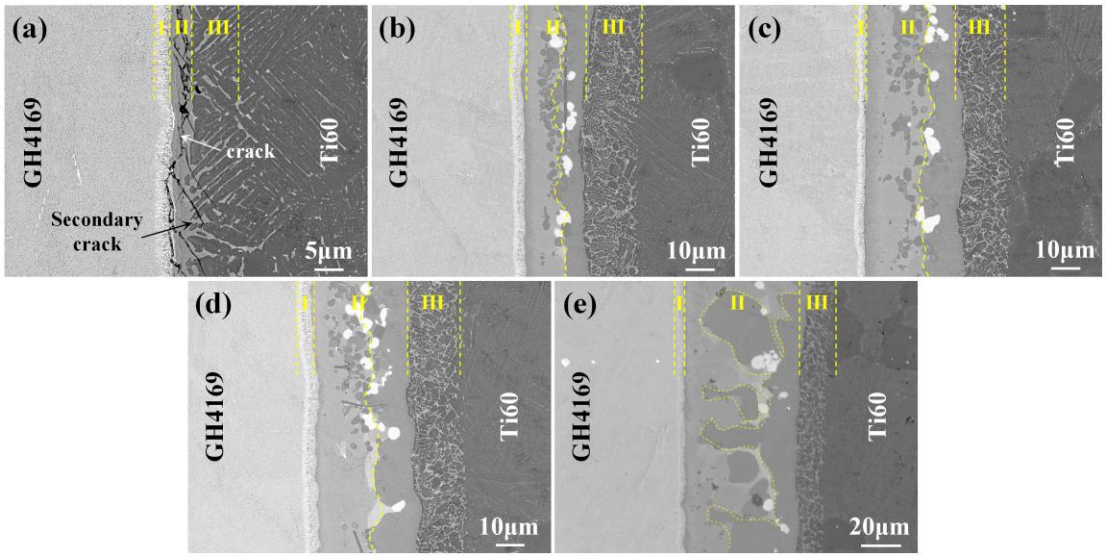


Figure 5. Microscopic morphology of GH4169/Ti60 joints diffusion bonded using Cu foils of different thicknesses, (a)0mm; (b)0.01mm; (c)0.03mm; (d)0.05mm; (e)0.1mm

3.3 EBSD analysis of joint microstructure

Figure 6 shows the grain size and crystallographic orientation of GH4169/Ti60 joints brazed with different Cu foil thicknesses, with Figure 6(a) - (c) presenting the inverse pole figure (IPF) maps of the joints. As shown in Figure 6(a), when no Cu foil is added, only interdiffusion of Ti

and Ni occurs in Zone I, which is a solid-state diffusion zone without a eutectic reaction; the grains in this zone are mainly columnar grains oriented along the <0001> direction[24]. Zone II consists of fine equiaxed grains, corresponding to the Ti_2Ni and TiNi compound layer. The grains in Zone III exhibit a growth direction perpendicular to the interface, similar to those in Zone I, and are oriented along the <01-10> direction. Figure 6(b) and (c) indicate that the addition of Cu foil hinders the solid-state diffusion between Ti and Ni and promotes the solid solution of Ni, resulting in smaller columnar grains in Zone I. The grain morphology in Zone II changes from round or elliptical grains at a Cu foil thickness of 0.03mm to coarse columnar and irregular grains at 0.1mm, with grains mainly growing along the <010> direction. The grains in Zone III also exhibit anisotropic characteristics[25].

From Figure 7(a、a1、a2), (b、b1、b2), and (c、c1、c2), it can be seen that when 0, 0.03mm, and 0.1mm Cu foils are added, the grains in the brazing seam grow anisotropically. The grain size in Zone I is relatively small and remains stable with increasing Cu content; the average grain size increases only from 0.61μm to 1.24μm, and the zone consists mainly of Ni-Cu solid solution. Zone II predominantly contains large grains, and its grain size varies significantly with increasing Cu thickness. At a Cu thickness of 0.03mm, the average grain size is 3.23μm, and the zone is mainly composed of the TiCu phase and the β-Ti + Ti_3Sn eutectic structure precipitated from the liquid during cooling. At a Cu thickness of 0.1mm, the average grain size increases to 10.59μm. This is because excessive Cu addition not only increases the amount of TiCu phase but also promotes the continuous growth of TiCu into the brazing seam, forming coarse phase clusters as shown in Figure 5(e)[26]. Zone III is the Ti-Cu interdiffusion layer, with a grain size distribution similar to that of Zone I. Large grains are scarce, and the average grain size does not exceed 2.30μm; the zone is mainly composed of α-Ti + TiCu. The increase in Cu thickness mainly affects the grain evolution in the brazing seam reaction layer, while its influence on the diffusion layers is limited.

Figure 8(a1) - (c1) show the distributions of low-angle grain boundaries (LAGBs) and high-angle grain boundaries (HAGBs) in the joints with different Cu foil thicknesses. As shown in Figure 8(a1), when no Cu foil is added, the brazing seam is dominated by HAGBs, with the highest proportion reaching 92.5%. At this stage, large residual stress exists in the brazing seam, and most grains are bonded only through limited atomic interactions. Dislocations could hardly accommodate the large misorientation between grains, so crack propagation could not be effectively impeded, which is consistent with the extensive cracking observed in the brazing seam described earlier. Compared with Figure 8(a1), when the Cu foil thickness is 0.03mm (Figure 8 b1), the number of LAGBs increases in all three zones. This is because the increased Cu content promotes the formation of the Cu-Ni solid solution and simultaneously facilitates the limited Ti-Cu reaction. Meanwhile, the increased proportion of LAGBs in Zone II leads to a higher dislocation density. Since the grain boundary energy increases with increasing

misorientation, the energy required for crack initiation in Zone II increases, making crack propagation more difficult[27]. As shown in Figure 8(c1), when the Cu foil thickness reaches 0.1mm, the number of LAGBs further increases. However, unlike the previous case, the LAGBs are mainly concentrated at the interface between Zone II and Zone III, i.e., adjacent to the Ti60 base metal. The fraction of HAGBs is 46.1%, and they are mainly concentrated near the GH4169 side. The increased Cu content promotes the diffusion of more Ni into the brazing seam to form TiNi compounds, inducing more lattice distortion and larger residual stress in the brazing seam, which facilitates crack initiation. This is consistent with the observation that fracture occurs in Zone II near the GH4169 side.

Figure 8 also shows the kernel average misorientation (KAM) distributions of the joints, which can be used to compare the residual stress levels at different positions of the joint[3]. As shown in Figure 8(a2) - (c2), in Zone I, the average KAM increases from 0.32° to 0.51° and the maximum KAM increases from 4.16° to 4.97° with increasing Cu foil thickness. The increased Cu content promotes the formation of a supersaturated Ni solid solution in the Zone I diffusion layer, thereby increasing lattice distortion. As shown in Figure 8(b2), at a Cu foil thickness of 0.03mm, the average KAM of Zone II is 0.23°. Although the maximum KAM reaches 4.99°, which is higher than that of the 0.1mm Cu foil joint shown in Figure 8(c2), the residual stress distribution in the brazing seam is relatively uniform, which effectively reduces stress concentration in the diffusion layers and suppresses crack initiation. As shown in Figure 8(c2), when a 0.1mm thick Cu foil is used, the residual stresses in Zones II and III are relatively high, with average KAM values of 0.63° and 0.65°, respectively. This originates from the excessively grown coarse TiCu phase clusters in the brazing seam mentioned above. The stress mismatch and lattice distortion between the Ni-supersaturated solid solution in the Zone I diffusion layer and the coarse TiCu phase clusters in Zone II are the main reasons for fracture occurring between the diffusion layer and the brazing seam.

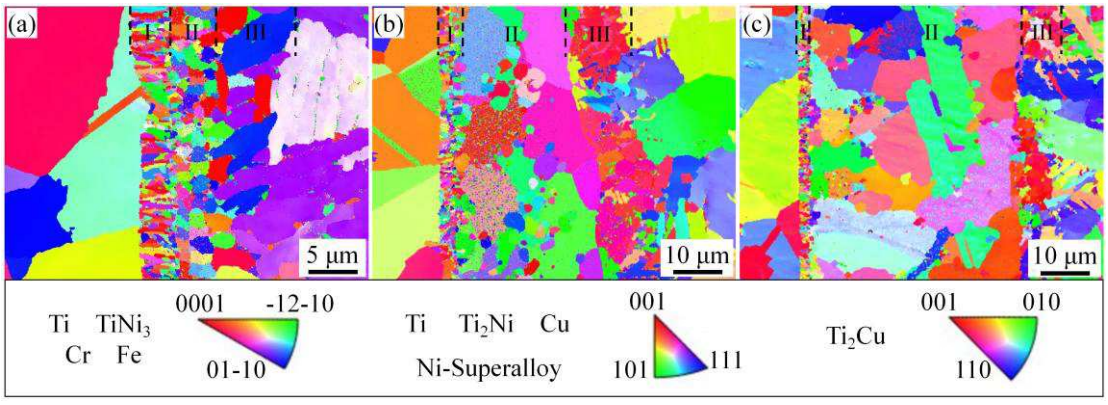


Figure 6. IPF results of GH4169/Ti60 joint interfaces diffusion-bonded using Cu foils of different thicknesses:

(a) 0mm; (b) 0.03mm; (c) 0.1mm

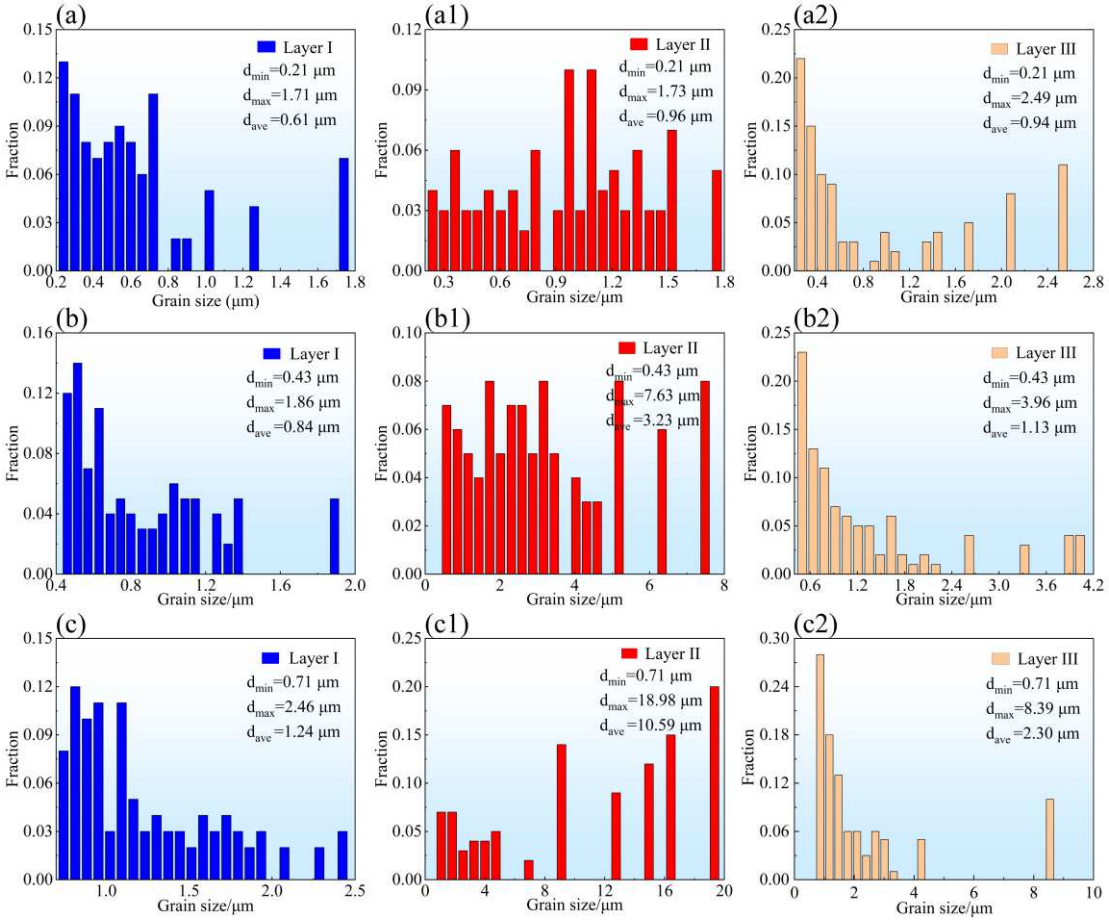


Figure 7. Effect of Cu foil thickness on grain size in different regions of GH4169/Ti60 joints

(a-a2) 0mm; (b-b2) 0.03mm; (c-c2) 0.1mm

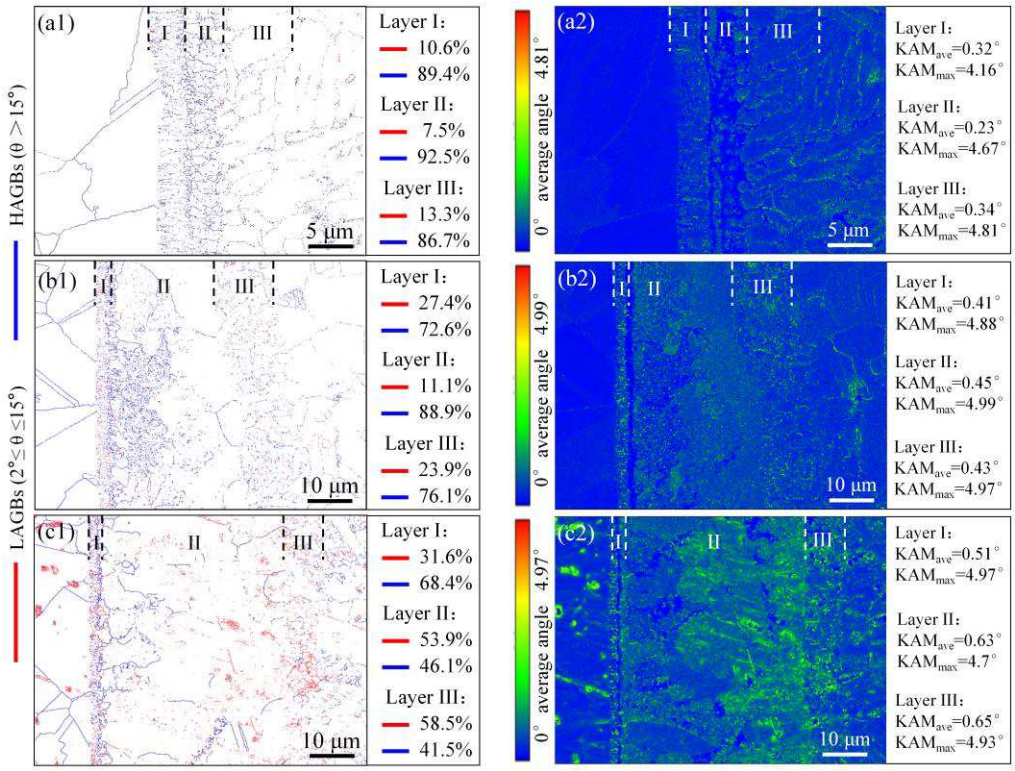


Figure 8. Effect of Cu foil thickness on the distribution of HAGBs/LAGBs and KAM in different regions of GH4169/Ti60 joints: (a1)(a2) 0mm; (b1)(b2) 0.03mm; (c1)(c2) 0.1mm

3.4 Mechanical properties of the joint

Figure 9 shows the shear strength of GH4169/Ti60 joints bonded with different Cu foil thicknesses. With increasing Cu foil thickness, the joint strength first increases and then decreases, reaching a maximum shear strength of 190MPa at a Cu foil thickness of 0.03mm. When GH4169/Ti60 is directly diffusion bonded without a Cu foil, the large stress mismatch between the base metals and the formation of brittle TiNi compounds result in a shear strength of only 16.2MPa. The addition of Cu foil hinders the direct interdiffusion of Ti and Ni, effectively suppressing the formation of brittle Ti-Ni compounds. At a Cu foil thickness of 0.03mm, the transition layer composed of $(Ni,Cr,Fe)_{ss}$/$(Cu,Ni)_{ss}$/Ti-Cu IMCs formed in the brazing seam greatly relieves the residual stress caused by the property mismatch between the base metals. The layered transition between the compound layers and solid solution layers results in the highest shear strength[28,29]. When the Cu foil thickness increases to 0.05mm and 0.1mm, the diffusion of Ti-Cu IMCs and more Ni into the center of the brazing seam disrupts the optimal phase layer distribution in the diffusion layers. Meanwhile, the excessive growth of brittle compound clusters also disrupts the optimal matching between different phase layers, leading to stress concentration in the joint as shown in Figure 8(c3). As a result, the joint performance deteriorates[30], and the shear strength is only 154.1MPa and 150MPa, respectively. This indicates that continuously increasing the Cu foil thickness does not always optimize the shear strength of the GH4169/Ti60 joint.

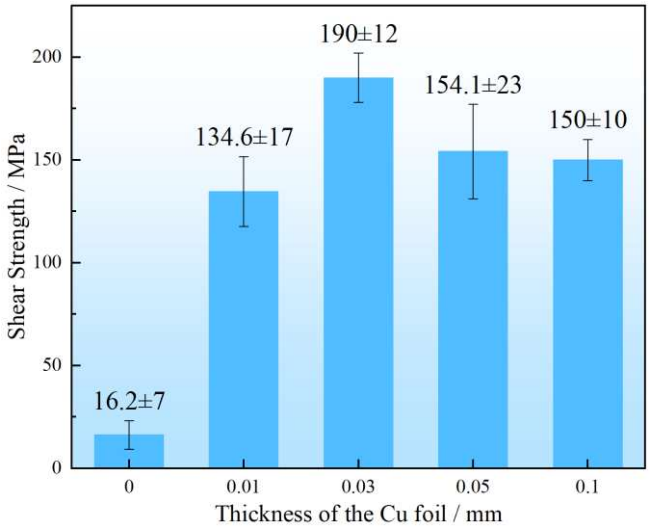


Figure 9. Effect of Cu foil thickness on the shear strength of GH4169/Ti60 joints

3.5 Analysis of joint fracture mode

Figure 10 and Figure 11 show the fracture morphologies and fracture paths of GH4169/Ti60 joints bonded with different Cu foil thicknesses, respectively. The results indicate that all joints failed in a brittle manner[31,32]. As shown in Figure 10 (a1) and (a2), when no Cu foil is added, the fracture surface exhibits a spalled morphology with distinct cleavage facets and continuous river patterns, indicating a typical cleavage fracture mode. As shown in Figure 11(a), (a1), (a2), fracture occurs in Zone II. Combined with the EDS analysis in Table 1, it can be inferred that fracture occurs between the Ti_2Ni and TiNi phases. As shown in Figure 11(c), (c1), (c2), when the Cu foil thickness increases to 0.03mm, the fracture location shifts from Zone II to the interface between the TiCu phase and $(Ni,Cr,Fe)_{ss}$ in Zone I, with only minor cracks generated in the brazing seam. The transition layer of "$(Ni,Cr,Fe)_{ss}$/$(Cu,Ni)_{ss}$/Ti-Cu IMCs" effectively relieves the stress mismatch in the brazing seam. The fracture surface exhibits smaller cleavage facets and discontinuous river patterns, indicating that the fracture mode changes from cleavage to quasi-cleavage fracture[23,33]. When the Cu foil thickness increases to 0.05mm and 0.1mm, fracture occurs in the brittle phase layer in Zone II. The fracture morphology shown in Figure 10 exhibits distinct cleavage steps, indicating typical transgranular brittle fracture. According to EDS analysis, the fracture surface mainly consists of Ti_2Cu, $TiAl_2$, and Ti_3Sn phases. Figure 11 also shows that many secondary cracks initiate at the fracture location and propagate from the Ti_2Cu and Ti_3Sn phases toward the α-Ti phase. This is because a large number of continuously distributed brittle compounds are dispersed in the center of the brazing seam, causing residual stress concentration and providing the driving energy for secondary crack propagation.

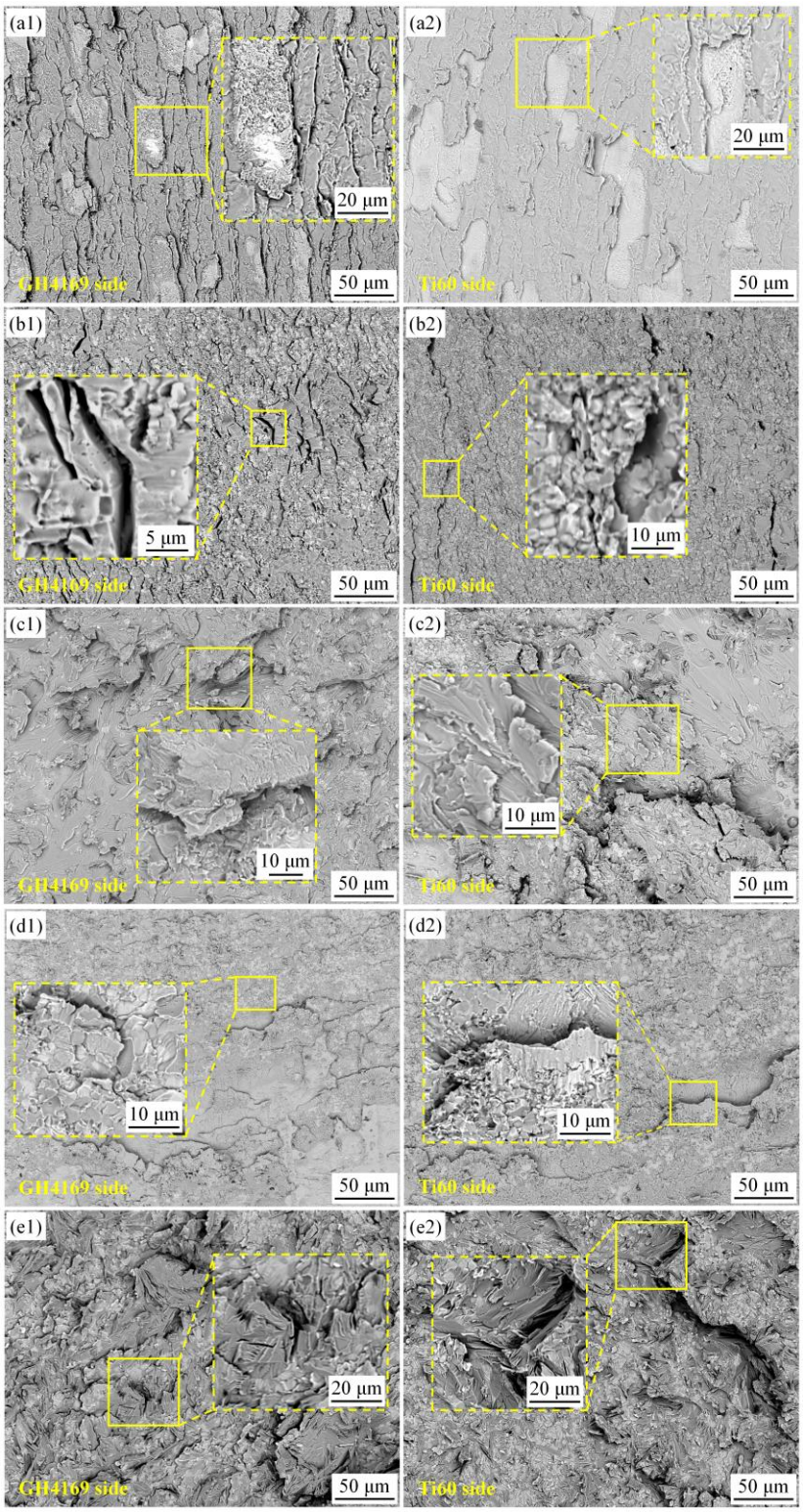


Figure 10. Fracture morphologies of GH4169/Ti60 joints with different Cu foil thicknesses

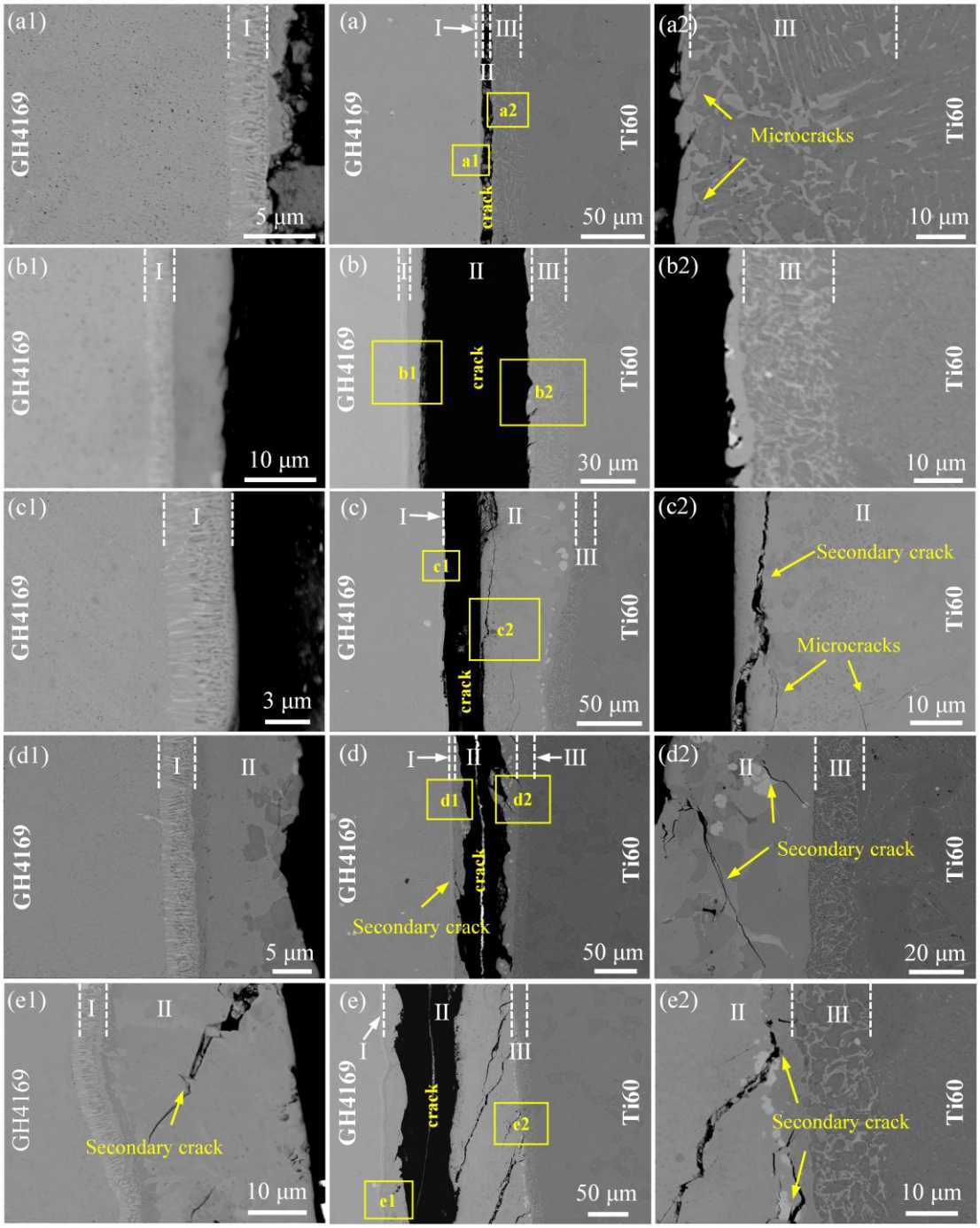


Figure 11. Fracture paths of GH4169/Ti60 joints with different Cu foil thicknesses

4. Conclusions

In this study, pure Cu foil was used as an interlayer to enhance the strength of Ti60/GH4169 dissimilar metal joints. The composition and ductility of intermetallic compounds (IMCs) in the joint were controlled by adjusting the thickness of the Cu interlayer. A bonded joint with excellent shear performance was ultimately obtained, providing a new interlayer design strategy for Ti/Ni dissimilar metal joining.

(1) The GH4169/Ti60 joint can be divided into three zones: diffusion reaction layers I and III adjacent to the GH4169 and Ti60 sides, respectively, and central brazing seam II. When a 0.03mm thick Cu foil is used as the interlayer, an interfacial microstructure of GH4169/Ti(Ni,Cu)/TiCu + TiAl/β-Ti + Ti_3Sn/α-Ti + Ti_2Cu/α-Ti/Ti60 is formed. The addition of Cu foil transforms the TiNi/Ti_2Ni phases in the brazing seam into β-Ti + TiCu phases.

(2) With increasing Cu foil thickness, the grains in Zones I and III are refined, whereas the grains in Zone II are relatively large and exhibit an anisotropic distribution. The fraction of high-angle grain boundaries (HAGBs) in Zone II decreases continuously, reaching 46.1% at a Cu foil thickness of 0.1mm. When the Cu foil thickness is 0.1mm, the average kernel average misorientation (KAM) values in Zones II and III reach their maximum values of 0.63° and 0.65°, respectively, indicating relatively high residual stress within the joint.

(3) The GH4169/Ti60 joint exhibits brittle fracture characteristics when no Cu foil is added, with cracks propagating along the TiNi phase. After the addition of Cu foil, the transition phase layer formed in the brazing seam hinders crack propagation, and fracture occurs between the TiCu phase and the β-Ti + Ti_3Sn phase. With increasing Cu foil thickness, the shear strength of the joint first increases and then decreases, reaching a peak value of 219.1MPa at a Cu foil thickness of 0.03mm.

References

[1] Y. Li, J. Qin, W. Long, S. Zhong, G. Zhang, P. Guo, Z. Ding, X. Chen, S. Wang, Review: high-temperature brazing in aerospace—challenges and filler metal optimization strategies for different joining systems, J Mater Sci 61 (2026) 27527–27564. https://doi.org/10.1007/s10853-026-13343-1.

[2] C. Xie, Microstructural evolution and mechanical properties of Ni-based superalloy joints brazed using a ternary Ni-W-B amorphous brazing filler metal, (2023).

[3] X. Hong, Insight into the performance of Ni_3Al/Ni interface regulated by vacancies stability via first-principles calculation, (2026).

[4] Z. Yu, W. Long, R. Qiu, S. Zhu, S. Yang, J. Qin, Y. Pei, T. Jiang, L. Zhang, H. Yu, In Situ Reaction of Cu/Zr Diffusion Bonded with GH4169/Ti60 Dissimilar Metal Joints, ACS Applied Engineering Materials (2026). https://doi.org/10.1021/acsaenm.6c00892.

[5] F. Khan, Recent Advances in High Entropy Alloy Fillers for Brazing Similar and Dissimilar Materials: A Review, (n.d.).

[6] Q. Zhao, Z. Qin, Y. Huang, P. Li, Z. Ding, L. Zhang, Y. Sun, J. Li, J. Liu, Q. Zhang, Y. Wang, H. Dong, Axial upset driven inertia friction welding of FGH4108/GH4065A dissimilar superalloys, The International Journal of Advanced Manufacturing Technology (n.d.).

[7] K. Han, Y. Cao, X. Jiang, Y. Xia, X. Wei, X. Zhang, X. Wei, Investigation on the microstructure and mechanical properties of TC4/GH4169 laser welded joint by novel V/Cu composite interlayer, Materials Letters 405 (2026) 139722. https://doi.org/10.1016/j.matlet.2025.139722.

[8] Y. Xia, G. Xu, Z. Pan, P. Li, Z. Ding, Y. Jiu, P. Guo, J. Qin, Q. Lu, X. Zhang, P. Zhou, S. Zhong, W. Long, The influence of Ni and Cu in Ti-based filler on the vacuum brazing of TiAl/GH4169 dissimilar alloys, Materials Characterization 231 (2026) 115934. https://doi.org/10.1016/j.matchar.2025.115934.

[9] P. Wang, Electric field suppresses intermetallics via enhanced diffusion and non-equilibrium phase transformation solid solution in ultrafast brazed Ti_2AlNb/Ti60 joints, (2026).

[10] Z. Yu, L. Zhang, Y. Sun, R. Qiu, H. Yu, Q. Gao, W. Long, Multiple Microstructure Evolution and Mechanical Properties of Gh4169/TC4 Brazed Joint, (2025). https://doi.org/10.2139/ssrn.5164593.

[11] H.S. Ren, H.P. Xiong, W.M. Long, Y.X. Shen, S.J. Pang, B. Chen, Y.Y. Cheng, Interfacial diffusion reactions and mechanical properties of Ti_3Al/Ni-based superalloy joints brazed with AgCuPd filler metal, Materials Characterization 144 (2018) 316–324. https://doi.org/10.1016/j.matchar.2018.07.024.

[12] Y. Wang, P. Li, L. Zhang, Z. Ding, C. Li, J. Li, X. Jiang, H. Dong, Multiscale microstructural consideration for high strength diffusion bonding of Ti_2AlNb alloy to GH4169 superalloy with $(TiZrHfNb)_{95}Al_5$ interlayer, Materials & Design 244 (2024) 113094. https://doi.org/10.1016/j.matdes.2024.113094.

[13] K. He, Q. Gao, L. Zhang, Pulse current diffusion bonding of high niobium β-γ TiAl alloy to IN718 superalloy by introducing pure Ni interlayer, Intermetallics 169 (2024) 108303. https://doi.org/10.1016/j.intermet.2024.108303.

[14] B. Wang, H. Shi, Z. Yu, P. Zhang, Q. Cheng, N. Song, H. Yan, Study on the microstructure

and mechanical properties of Ti-Zr-Cu-Ni amorphous filler brazed Inconel 718 and 3D printed TC4 alloy, Weld World 67 (2023) 455–471. https://doi.org/10.1007/s40194-022-01411-4.

[15] S. Simões, C.J. Tavares, A. Guedes, Joining of γ-TiAl Alloy to Ni-Based Superalloy Using Ag-Cu Sputtered Coated Ti Brazing Filler Foil, Metals 8 (2018) 723. https://doi.org/10.3390/met8090723.

[16] Effects of Brazing Filler Composition and Brazing Temperature on the Microstructure and Mechanical Properties of Ti_2AlNb and GH4169 Alloy Brazed Joints, Journal of Mechanical Engineering 60 (2024) 116. https://doi.org/10.3901/JME.2024.22.116.

[17] A. Babaei-Dehkordi, M. Soltanieh, M. Mirjalili, A. Mostafaei, Quantitative analysis of diffusion kinetics of intermetallic formation in Ni–Ti system, Journal of Materials Research and Technology 20 (2022) 4545–4555. https://doi.org/10.1016/j.jmrt.2022.09.017.

[18] L. Zhang, H. Dong, P. Li, S. Li, B. Wu, Y. Ma, L. Huang, C. Li, J. Li, Y. Yang, Vacuum brazing TiAl intermetallic to K4169 alloy using amorphous filler metals $Ti_{56.25-x}Zr_x$-$Ni_{25}Cu_{18.75}$, Journal of Materials Science & Technology 154 (2023) 217–231. https://doi.org/10.1016/j.jmst.2022.12.073.

[19] J. Cai, S. Hu, H. Liu, D. Lin, W. Fu, X. Song, Microstructural Evolution and Mechanical Properties of Ti_2AlNb/GH99 Superalloy Brazed Joints Using TiZrCuNi Amorphous Filler Alloy, Aerospace 10 (2023) 73. https://doi.org/10.3390/aerospace10010073.

[20] P. Wang, Microstructure evolution, interfacial bonding and surface energy mechanism of Ti_2AlNb/Ti60 brazed joint with Cu/Ni-free Ti-Co-Fe-Sn amorphous filler, (2026).

[21] Y. Bai, Strengthening the diffusion bonding of Zr-4 alloys through regulating surface roughness and Ti interlayer thickness, (2025).

[22] P. Wang, Homogenization treatment-induced reduction of brittle intermetallic compounds in Ti_2AlNb/Ti60 brazed joints: Effect on microstructure and mechanical properties, Materials Science (2024).

[23] P. Wang, Enhancement of mechanical properties in Ti_2AlNb/Ti60 brazed joints via Nb foam-induced in-situ formation of tough Ti4Nb phase, (2024).

[24] Z. Zhai, X. Ren, H. Ren, H. Xiong, W. Li, Y. Shang, Y. Cheng, Dissimilar joining of TiAl alloy to Ni-based superalloy using a Ni-Co-Fe-Mn-Cr-Ge-(Si, B) high-entropy alloy as brazing filler metal, Weld World 70 (2026) 2315–2327. https://doi.org/10.1007/s40194-025-02237-6.

[25] D. Dong, K. Shi, D. Zhu, Y. Liang, X. Wang, Z. Wei, J. Lin, Microstructure evolution and mechanical properties of high Nb–TiAl alloy/GH4169 joints brazed using CuTiZrNi amorphous filler alloy, Intermetallics 139 (2021) 107351. https://doi.org/10.1016/j.intermet.2021.107351.

[26] W. Zhang, L. Zhang, Z. Yu, D. Shang, T. Jiang, Z. Liao, Y. Lv, Q. Gao, X. Liu, K. Li, Y. Zhou, S. Zhong, Y. Pei, H. Yu, Effect of Nb content on microstructure and mechanical properties in TiAl/Ti_2AlNb alloy joint vacuum brazed with $Ti_{50-x}Zr_{12.5}Hf_{12.5}Cu_{25}Nb_x$ filler metal, International Journal of Refractory Metals and Hard Materials 142 (2027) 108089. https://doi.org/10.1016/j.ijrmhm.2026.108089.

[27] X. Li, J. Lin, P. Lin, S. Zhang, X. Zhang, F. Lu, C. Wang, T. Lin, P. He, High-density dislocation and ductile precipitate synergistically reinforced TiAl/Ni-based superalloy joint

using novel multi-principal element interlayer, Journal of Materials Science & Technology 183 (2024) 193–205. https://doi.org/10.1016/j.jmst.2023.09.058.

[28] L. Zhang, P. Li, H. Dong, Dispersion, solid solution, and covalent bond coupled to strengthen K4169/TiAl composite brazed joints: First-principles and experimental perspective, Journal of Materials Science & Technology 218 (2025) 287–304. https://doi.org/10.1016/j.jmst.2024.08.050.

[29] L. Zhang, M. Ran, Q. Chang, C. Ding, B. Zhang, B. Zhang, Z. Sun, Microstructure and mechanical properties of a TiAl/GH3039 joint brazed with a Ti-Zr-Nb-Ni-Cu-Co high-entropy alloy filler, Materials Characterization 240 (2026) 116953. https://doi.org/10.1016/j.matchar.2026.116953.

[30] L. Li, W. Zhao, Z. Feng, J. Sun, X. Li, Microstructure and shear strength of γ-TiAl/GH536 joints brazed with Ti−Zr−Cu−Ni−Fe−Co−Mo filler alloy, Transactions of Nonferrous Metals Society of China 30 (2020) 2143–2155. https://doi.org/10.1016/S1003-6326(20)65367-5.

[31] S. Li, Z. Liu, Y. Xia, X. Wang, P. He, Y. Jiu, L. Jia, W. Long, Vacuum brazing TiAl intermetallics to GH3030 alloy with a multi-component Ti-based filler metal, Journal of Manufacturing Processes 70 (2021) 484–493. https://doi.org/10.1016/j.jmapro.2021.09.001.

[32] B. Wan, X. Li, C. Pan, D. Li, S. Qu, C. Yang, Microstructure and mechanical properties of TiAl/Ni-based superalloy joints vacuum brazed with Ti–Zr–Fe–Cu–Ni–Co–Mo filler metal, Rare Metals 40 (2021) 2134–2142. https://doi.org/10.1007/s12598-020-01550-x.

[33] T. Zhang, Microstructure evolution and brazing mechanism of Ti_5Si_3/Ti_3Al composite and Ni-based superalloy joints using Ti-Zr-Cu-Ni filler alloy, (2018).

[34] Y. Wang, Z. Ding, B. Wang, Z. Zhang, Z. Qin, J. Yao, Y. Sun, F. Yu, H. Dong, P. Li, A high-entropy gradient filler metal enables high-strength joints of Ti_2AlNb and GH4169 alloys, Mater. Horiz. 13 (2026) 3057–3068. https://doi.org/10.1039/D5MH02009C.

[35] Y. Wang, Vacuum brazing of Ti_2AlNb and TC4 alloys using Ti–Zr–Cu–Ni and Ti–Zr–Cu–Ni+Mo filler metals: Microstructural evolution and mechanical properties, (n.d.).

Supplementary Files

This is a list of supplementary files associated with this preprint. Click to download.

- DeclarationofInterestStatement.docx